Terra Nova

doi: 10.1111/ter.12231

Multi-phase late-Neogene exhumation history of the Aar massif, Swiss central Alps

Pierre G. Valla,[1,2] Meinert Rahn,[3,4] David L. Shuster[5,6] and Peter A. van der Beek[7]

[1]*Institute of Earth Surface Dynamics, University of Lausanne, Lausanne CH-1015, Switzerland;* [2]*Department of Earth Sciences, ETH Zürich, Zürich CH-8092, Switzerland;* [3]*Swiss Federal Nuclear Safety Inspectorate, Brugg CH-5200, Switzerland;* [4]*Department of Mineralogy and Geochemistry, University of Freiburg, Freiburg D-79104, Germany;* [5]*Department of Earth & Planetary Science, University of California, Berkeley, CA 94720, USA;* [6]*Berkeley Geochronology Center, Berkeley, CA 94707, USA;* [7]*Institute of Earth Sciences (ISTerre), Université Grenoble Alpes, Grenoble F-38400, France*

ABSTRACT

The late-Neogene evolution of the European Alps was influenced by both tectonic and climatically driven erosion processes, which are difficult to disentangle. We use low-temperature thermochronometry data from surface and borehole samples in the Aar massif–Rhône valley (Swiss central Alps) to constrain the exhumation history of the region. Multiple exhumation events are distinguished and linked to regional-scale tectonic deformation (before 5 Ma), short-lived climatically driven orogen contraction (between 4 and 3 Ma), and glacial valley carving since *c*. 1 Ma. Compared with previous studies, we clearly show the existence of two separate exhumation phases in the Late Miocene–Pliocene and better constrain the onset of glacial valley carving. The hydrothermal activity and geothermal anomalies currently observed in the borehole have been local and short-lived, with only a minor influence on thermochronometric observations. We thus suggest that late-stage glacial valley carving may have triggered topography-driven fluid flow and transient hydrothermal circulation.

Terra Nova, 00: 1–12, 2016

Introduction

Quantifying mountain evolution, as well as sediment transfer to surrounding basins, is important for understanding potential feedbacks between climate, erosion and tectonics (e.g. Molnar and England, 1990; Raymo and Ruddiman, 1992). However, those couplings are difficult to decipher because the involved processes are often interrelated (Roe *et al*., 2008; Whipple, 2009), promoting transient erosion or topographic response (Willett and Brandon, 2002; Whipple and Meade, 2006). The late-Neogene evolution of the European Alps is a classic illustration of such a debate (see review in Willett, 2010). Sediment budgets from basins surrounding the Alps suggest a significant increase in accumulation rates since *c*. 5 Ma (Kuhlemann *et al*., 2002), roughly concordant with (1) the onset of denudation in the northern Alpine foreland basin (Cederbom *et al*., 2004, 2011), (2) increased Alpine exhumation (Vernon *et al*., 2008) and (3) potential migration of deformation from the frontal Jura (Becker, 2000) to the internal parts of the belt (Willett *et al*., 2006). However, exhumation histories across the European Alps have led to contrasting conclusions concerning the existence and precise timing of this increase, as well as the nature of the forcing processes. Ongoing tectonic deformation and crustal accretion (Persaud and Pfiffner, 2004; Schlunegger and Mosar, 2011), orogen-perpendicular extension (e.g. Reinecker *et al*., 2008; Cardello *et al*., 2015) and regional-scale slab unloading (Baran *et al*., 2014; Fox *et al*., 2015) have been proposed as potential tectonic triggers. Drainage rearrangement leading to river capture and transient incision has also been proposed (Ziegler and Fraefel, 2009; Schlunegger and Mosar, 2011; Yanites *et al*., 2013). Alternatively, climatic processes have been suggested, including a transition to wetter conditions (Cederbom *et al*., 2004, 2011; Willett *et al*., 2006) or the (more recent) impact of Pliocene–Quaternary glaciation (Haeuselmann *et al*., 2007; Glotzbach *et al*., 2011; Valla *et al*., 2011, 2012; Mahéo *et al*., 2012; Fox *et al*., 2015). Better temporal constraints on bedrock exhumation should help to elucidate which processes were the primary drivers of the late-stage Alpine evolution.

In this study, we apply multiple low-temperature thermochronometric systems to bedrock samples along both a 2 km surface elevation profile and a 500 m deep borehole in the Swiss central Alps. Our objective is to quantitatively constrain the late-Neogene exhumation history of the region and assess the potential climatic or tectonic controls on it.

Setting and methods

The Visp-Brigerbad area lies in the upper Rhône valley between the crystalline Aar massif and the sedimentary Helvetic and Penninic nappes (Fig. 1). It encompasses two major tectonic boundaries: the Penninic frontal thrust (PFT) and the Rhône-Simplon fault (RSF) (Mancktelow, 1985, 1992; Seward and Mancktelow, 1994; Campani *et al*., 2010). The modern drainage pattern follows the tectonic structures (Kühni and Pfiffner, 2001), influenced by the exhumation of the External Crystalline Massifs (ECMs) since Oligocene–Early Miocene times (Schmid *et al*., 2004), while the overall high Alpine elevation has been acquired at least since Miocene times (Campani *et al*., 2012). The current kinematics of the

Correspondence: Pierre G. Valla, Institute of Earth Surface Dynamics, University of Lausanne, Lausanne CH-1015, Switzerland. E-mail: pierre.valla@unil.ch

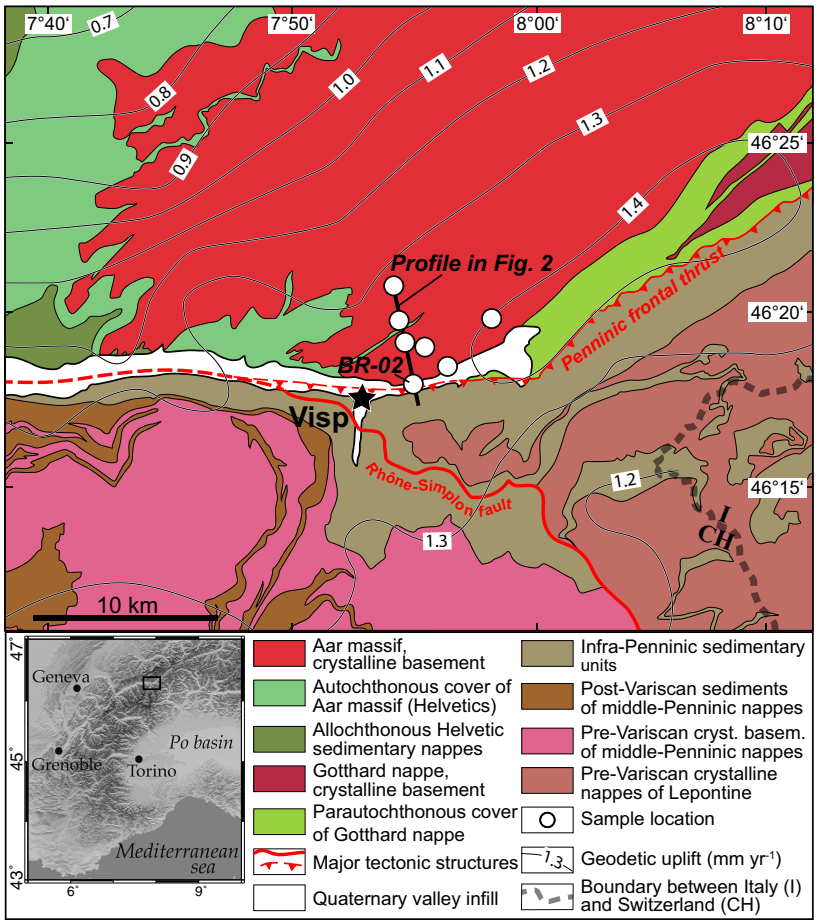

Fig. 1 Geological sketch map of the Swiss central Alps (after Schmid *et al.*, 2004) with main litho-tectonic units and major tectonic structures (see legend). White circles represent sampling locations (BR-02 is the geothermal borehole, see Fig. 7B), the thick black line indicates the cross-section shown in Fig. 2A, and thin black lines depict surface-uplift rates from geodetic measurements with respect to Laufenburg (Schlatter, 2014). Inset shows the location of the study area within the European Alps.

central Swiss Alps show no active convergence (Nocquet and Calais, 2004) but evidence for orogen-parallel extension (Champagnac *et al.*, 2004). The area shows a strong glacial imprint with high topographic relief and glacially shaped cross-profiles along the Rhône valley (Norton *et al.*, 2010). This valley has been glacially deepened during Quaternary times (Valla *et al.*, 2011), with large glacial overdeepenings (Finckh and Frei, 1991; Rosselli and Olivier, 2003) filled by post-glacial sediments (Hinderer, 2001). Average Quaternary and Holocene erosion patterns (Champagnac *et al.*, 2007, 2009) closely correlate with surface-uplift rates of up to >1 mm a^{-1} in the upper Rhône valley (Fig. 1). Hydrothermal springs and geothermal anomalies occur along the Rhône valley, apparently associated with major tectonic structures (e.g. Sonney and Vuataz, 2008, 2009). The importance and persistence of these hydrothermal systems remain poorly constrained.

We use low-temperature apatite (U–Th–Sm)/He (AHe) and fission-track (AFT) thermochronometry, including fission-track length (TL) measurements, to quantify the late-Neogene exhumation history of the area. The AHe and AFT systems are characterised by closure temperatures of 50–90 °C (Shuster *et al.*, 2006) and 100–120 °C (Gallagher *et al.*, 1998), respectively, and are sensitive to topographic changes (e.g. Stüwe *et al.*, 1994; Braun, 2002). Geothermal anomalies and topography-driven hydrothermal circulation may also affect low-temperature thermochronometers (Ehlers, 2005; Dempster and Persano, 2006; Whipp and Ehlers, 2007); this sensitivity can help in assessing the persistence of near-surface geothermal systems (e.g. Gorynski *et al.*, 2014). Here, we combine six surface samples (VIS) collected along an elevation profile (Valla *et al.*, 2011) with three new samples (MRP) obtained along a 500 m deep geothermal borehole, covering ~3 km elevation in total (Table 1). AHe ages for the VIS samples have been previously reported (Valla *et al.*, 2011). We report here new AFT data including TL distributions for all VIS and MRP samples (Table 2) and

Table 1 Sample locations for the elevation profile from the Gärsthorn to Visp-Brigerbad (VIS), with additional samples from the Brigerbad geothermal borehole (MRP). Asterisks mark samples from Valla *et al.* (2011). All sampled rocks are orthogneisses from the Aar crystalline basement.

Sample	Longitude (°E)	Latitude (°N)	Elevation (m) (depth below valley floor)
VIS-01*	7.91667	46.34390	2925
VIS-03*	7.92035	46.32918	2100
VIS-04*	7.92432	46.31988	1600
VIS-05*	7.93780	46.31788	1400
VIS-06*	7.98339	46.32999	850
VIS-07*	7.95333	46.30967	670
MRP-424	7.93032	46.30220	487 (−167)
MRP-425	7.93032	46.30220	321 (−333)
MRP-426	7.93032	46.30220	157 (−497)

Apatite grains were extracted from crushed bedrock samples using standard magnetic and heavy-liquid separation techniques.

Table 2 Apatite fission-track data of VIS and MRP samples.

Sample *N*° and locality	Elevation (m)	Mineral (No. crystals)	Spontaneous ρs (Ns)	Induced ρi (N_i)	$P\chi^2$	Dosimeter ρd* (N_d)	Central FT Age (Ma) (−2σ/+2σ)	Mean TL (μm)	SD of TL distribution (No. tracks)	Mean Dpar (SD)
VIS-01 Gärsthorn	2925	Apatite (25)	0.011 (274)	0.483 (11561)	98%	15.63 (7989)	6.4 (−0.4/+0.4)	14.24	1.20 (67)	1.80 (0.13)
VIS-03 Bischeru	2100	Apatite (40)	0.008 (318)	0.347 (13793)	100%	15.63 (7991)	6.2 (−0.4/+0.4)	14.21	1.17 (87)	1.91 (0.16)
VIS-04 Bodma	1600	Apatite (40)	0.005 (178)	0.281 (10444)	94%	15.63 (7993)	4.6 (−0.3/+0.4)	13.76	1.58 (70)	1.96 (0.15)
VIS-05 Tähischinu	1400	Apatite (40)	0.003 (135)	0.193 (7940)	22%	15.64 (7996)	4.6 (−0.4/+0.4)	13.87	1.27 (44)	1.90 (0.17)
VIS-06 Chilchmatte	850	Apatite (40)	0.005 (201)	0.380 (15971)	100%	15.64 (7998)	3.4 (−0.2/+0.3)	14.26	1.28 (100)	1.82 (0.16)
VIS-07 Gamsen	670	Apatite (40)	0.004 (201)	0.373 (18249)	96%	15.65 (8000)	3.0 (−0.2/+0.2)	13.79	1.11 (29)	1.94 (0.20)
MRP-424 Brigerbad, −167 m	487	Apatite (40)	0.004 (182)	0.421 (17047)	100%	15.65 (8002)	2.9 (−0.2/+0.2)	13.36	1.29 (72)	2.77 (0.21)
MRP-425 Brigerbad, −333 m	321	Apatite (40)	0.003 (106)	0.367 (11848)	100%	15.66 (8004)	2.4 (−0.2/+0.2)	13.02	1.77 (27)	2.91 (0.33)
MRP-426 Brigerbad, −497 m	157	Apatite (40)	0.001 (38)	0.135 (5729)	88%	15.66 (8006)	1.8 (−0.3/+0.3)	12.84	2.25 (18)	2.22 (0.21)

(i) Apatite grains were mounted with epoxy on glass slides, polished, and etched at 21°C for 20 s with 5N HNO_3 to reveal spontaneous fission tracks. Mounts were then covered with U-free white mica sheets and sent to irradiation at the FRM-II reactor (Garching, Germany), together with CN5 dosimeter glasses. After irradiation, white micas were etched for 45 min in 40% HF to reveal induced tracks. (ii) Fission tracks were counted and confined track lengths measured using transmitted light at 1600× magnification on a Zeiss Axioplan microscope (Basel University, Switzerland). Central ages (Galbraith and Laslett, 1993) and 2σ errors were calculated using the IUGS-recommended zeta calibration approach (Hurford and Green, 1983). (iii) Track densities are ($\times 10^7$ tr cm^{-2}), * = ($\times 10^5$ tr cm^{-2}) with numbers of tracks counted (N_d) shown in brackets. (iv) Analysis by external-detector method using 0.5 for the $4\pi/2\pi$ geometry correction factor (e.g. von Hagke *et al.*, 2012). Ages calculated using dosimeter glass CN-5 for apatite with $\zeta_{CN5} = 344 \pm 5$. (v) $P\chi^2$ is probability of obtaining χ^2 value for v degrees of freedom (v = number of crystals - 1). All samples passed the statistical χ^2 tests indicating that single-grain ages belong to one single age population. Track length (TL) and Dpar data are given in 10^{-6} m, SD = 1σ standard deviation. Dpar measurements indicate elevated Cl contents for the borehole samples (MRP).

Table 3 Apatite (U–Th–Sm)/He data for MRP samples (Brigerbad geothermal borehole). See Valla *et al.* (2011) for analytical details of VIS samples.

Sample *N*°	^{238}U (nmol g^{-1})	^{232}Th (nmol g^{-1})	^{147}Sm (nmol g^{-1})	^{4}He (nmol g^{-1})	Raw age (Ma)	F_T	Corrected age (Ma)
MRP-424_y	132.3	222.8	211.4	0.159	0.67	0.72	0.94
MRP-424_z	95.4	201.0	221.1	0.083	0.45	0.719	0.63
MRP-424_t	106.4	252.1	245.1	0.090	0.42	0.70	0.61
MRP-424_v	135.4	199.7	181.1	0.185	0.79	0.72	1.1
MRP-424							**0.82 ± 0.24**
MRP-425_z	135.9	234.0	283.5	0.210	0.85	0.678	1.27
MRP-425_t	159.0	268.9	353.4	0.100	0.35	0.651	0.54
MRP-425_v	97.9	204.6	405.2	0.066	0.35	0.637	0.55
MRP-425							**0.79 ± 0.42**
MRP-426_x	64.5	49.3	514.8	0.032	0.31	0.802	0.39
MRP-426_y	81.9	46.9	489.6	0.047	0.38	0.769	0.49
MRP-426_z	46.9	26.7	246.8	0.028	0.40	0.691	0.58
MRP-426_v	74.4	62.3	297.8	0.053	0.45	0.667	0.68
MRP-426							**0.54 ± 0.12**

(i) Preparation included selection of grains with euhedral shape, uniform size and absence of inclusions. (ii) Single-crystal aliquots of apatite were wrapped in Pt foils and degassed by laser heating (Tremblay *et al.*, 2015) under ultra-high vacuum using a feedback-controlled 70-W diode laser at the Noble Gas Thermochronometry Laboratory of the Berkeley Geochronology Center, USA. ^4He abundances were measured by isotope dilution with ^3He using a quadrupole mass spectrometer operated in static vacuum mode. Degassed aliquots were dissolved and U, Th and Sm concentrations were measured by isotope dilution using an ICP-MS. Analytical uncertainties are <1, ~3 and ~2% for U, Th and Sm measurements respectively; and <1% for ^4He measurements. (iii) An α-ejection correction (F_T = the fraction of alpha particles produced within the crystal) was applied to calculate the (U–Th–Sm)/He age following Farley *et al.* (1996). Bold numbers are mean ages calculated from the replicates; 1σ error for mean ages is standard deviation of replicate ages. Replicate analyses of Durango apatite yielded a <5% reproducibility compared to the reference age.

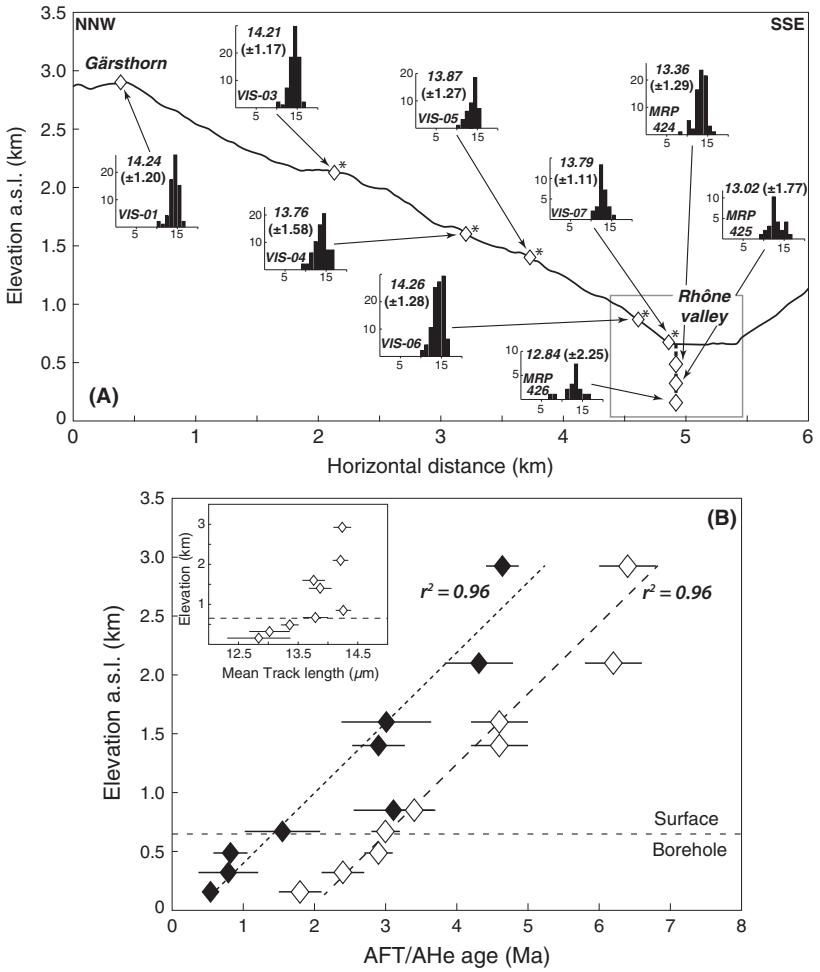

Fig. 2 Topographic cross-section and apatite (U–Th–Sm)/He and fission-track data. (A) Valley cross-section (see Fig. 1 for location) and apatite fission-track length histograms (including mean track length ± standard deviation) for VIS and MRP samples projected onto the section line (open diamonds with * indicate samples with $^4He/^3He$ data discussed in Valla *et al.*, 2011). The lower right rectangle outlines the extent of Fig. 7A. (B) Age–elevation profiles for apatite fission-track (AFT, open diamonds) and (U–Th–Sm)/He (AHe, black diamonds) ages from surface and borehole samples. Inset shows mean fission-track lengths (± standard error of the mean). Weighted linear fits to the data (dotted line: AHe ages; dashed line: AFT ages) suggest apparent steady Pliocene–Quaternary exhumation at ~0.6–0.7 km Ma^{-1}.

supplementary AHe ages for the MRP samples (Table 3).

Thermal modelling was initially performed on individual samples using HeFTy software (Ketcham, 2005). We used single-grain AFT ages and TL distributions (including *c*-axis angle correction; Ketcham *et al.*, 2007a) with Dpar values calibrated to standard values for deriving grain-specific annealing models (Ketcham *et al.*, 2007b). AHe ages were modelled using mean uncorrected AHe ages (Ketcham *et al.*, 2011), averaged grain size and U–Th–Sm content and diffusion kinetics based on the RDAAM algorithm (Flowers *et al.*, 2009). Inverse models used the present-day sample temperature (±5 °C) and large time–temperature boxes around the thermochronometric ages to maximise exploration of the thermal history space (Figs. 3 and 4). We subsequently used a similar approach with QTQt software (Gallagher, 2012), but combining all VIS and MRP datasets, to quantitatively constrain a single regional cooling history (i.e. common to all samples) and geothermal gradient that best predicts all the data in a consistent manner (Figs. 5 and S1 for details).

Results

Surface (VIS) and borehole (MRP) samples show AFT and AHe ages of 1.8–6.5 Ma and 0.5–4.5 Ma respectively (Fig. 2B). From the age–elevation relationships, an apparent exhumation rate of ~0.6–0.7 km Ma^{-1} may be derived from both AFT and AHe ages, suggesting steady exhumation since the late Neogene. Track lengths for VIS samples are relatively long (mean TL ~14 μm) with low dispersion, while borehole (MRP) samples are associated with shorter (mean TL ~13 μm) and more dispersed TL distributions (Fig. 2A). However, the latter are potentially biased by the relatively low number of measured track lengths for MRP-425 and MRP-426 (<50, Table 2) and should thus be interpreted with caution.

HeFTy modelling of individual samples reveals a complex late-Neogene cooling history for the area

Fig. 3 Modelled time–temperature paths for VIS samples (A: VIS-01; B: VIS-03; C: VIS-04; D: VIS-05; E: VIS-06; F: VIS-07) using HeFTy software (Ketcham, 2005). Black lines represent thermal histories with 'good' fit to the data (average goodness-of-fit value for all constraints >0.5); grey lines define thermal histories with 'acceptable' fit to the data (average goodness-of-fit value for all constraints >0.05; Ketcham *et al.*, 2009). Light-grey rectangles are initial model constraints placed around the thermochronometric ages; red stars mark present-day mean annual surface temperatures. Random subsegment spacing was used and no continuous cooling constraint was applied. Modelling was run until 500 'good' fits were obtained. First modelling iterations (not shown here) encompassed the full time–temperature domain so as not to guide predicted thermal histories. Model constraints were progressively reduced around time–temperature regions derived during the first iterations. Modelling results are not sensitive to reducing the model constraints, but this approach maximizes thermal history exploration in regions allowed by the thermochronometric data.

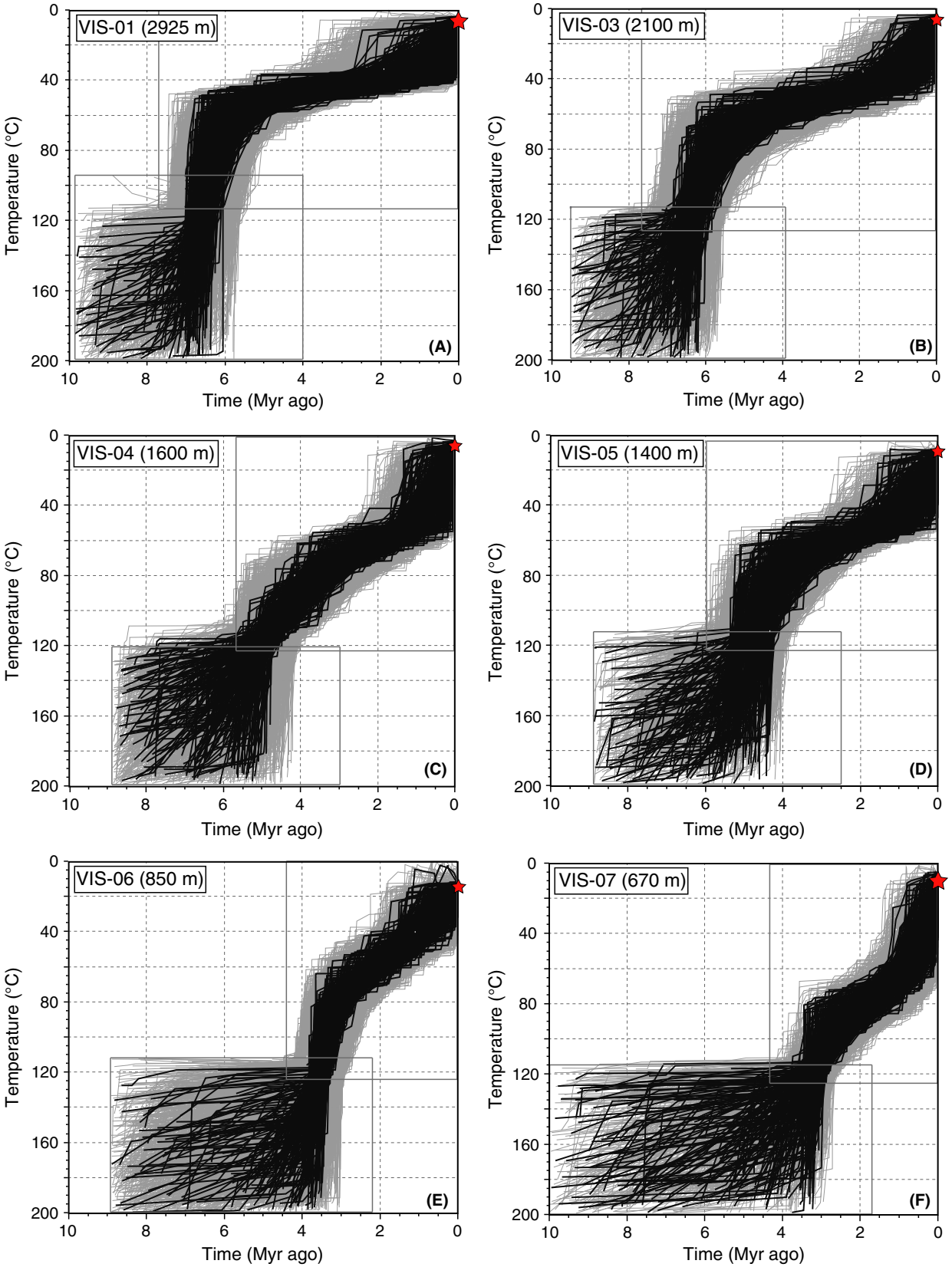

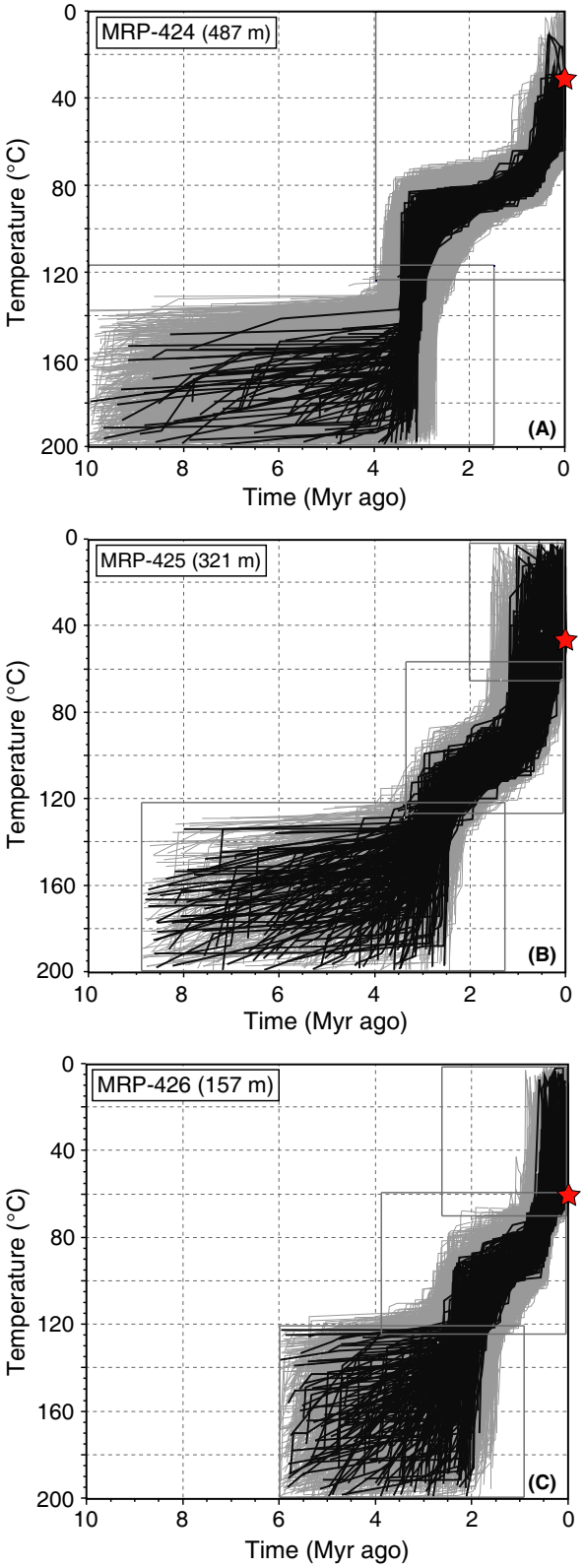

Fig. 4 Modelled time–temperature paths for MRP borehole samples (A: MRP-424; B: MRP-425; C: MRP-426) using HeFTy software (Ketcham, 2005). Red stars mark present-day measured temperatures in the borehole (Alpgéo/Norbert, 2011). The significance of line colours, boxes and the modelling approach are explained in the Fig. 3 caption.

(Figs. 3 and 4). High-elevation samples suggest rapid cooling until ~6–5 Ma (our data cannot constrain the onset of this phase, Fig. 3A,B), while lower samples indicate a later cooling event between *c.* 4 and 3 Ma (Fig. 3E,F). The late-stage history is characterised by rapid cooling since *c.* 1 Ma for low-elevation and borehole samples (Figs. 3F and 4). All samples are from the Aar massif, with no significant fault identified between sample locations and no AFT age-offset at a more regional scale (Fig. 6). They should thus share a common cooling history, which we quantitatively constrained using QTQt modelling (Fig. 5). Output results confirm a multi-step cooling history (based on a palaeo-geothermal gradient of ~26–28 °C km^{-1} predicted from QTQt modelling) including the following exhumation phases: (1) before 5 Ma at ~1 km Ma^{-1}, (2) a pulse at ~1.5 km Ma^{-1} between 4 and 3 Ma and (3) spatially variable exhumation since 1–0.8 Ma (i.e. from <0.1 km Ma^{-1} for VIS-01 up to >1.5 km Ma^{-1} for VIS-07, Fig. 5) associated with an increase in the geothermal gradient. Finally, we used each individual sample's apatite partial annealing zone (APAZ ~60–120 °C, i.e. in which information on cooling is recorded by AFT and TL data, Fig. S3) to link relevant AFT time slices from HeFTy modelling into a common time–temperature path, allowing us to qualitatively estimate a shared palaeo-geothermal gradient. We obtained maximum overlap with palaeo-geothermal gradients of 30 ± 5 °C km^{-1} (Fig. S4), in agreement with QTQt modelling results.

Discussion

Our extensive thermochronometric dataset reveals the late-Neogene exhumation history of the Aar massif. Both AFT and AHe age–elevation relationships suggest steady exhumation at ~0.6–0.7 km Ma^{-1} (Fig. 2B). However, this apparent exhumation rate may have been affected by large-scale topographic changes, such as glacial valley deepening/widening (e.g. Braun, 2002; Densmore *et al.*, 2007; Valla *et al.*, 2010; Olen *et al.*, 2012), and, therefore, cannot be taken at face value.

Previous studies using ^{4}He/^{3}He thermochronometry on VIS samples

(Fig. 2, Valla *et al.*, 2011) and compiling regional AFT and AHe data (Valla *et al.*, 2012) came to different conclusions about the late-Neogene exhumation history of the area. Both studies proposed late-stage differential exhumation histories between high- and low-elevation samples, which were interpreted as a record of glacial valley carving (Valla *et al.*, 2011). The $^{4}He/^{3}He$ data constrained the time of onset of this phase of major relief increase to be between 0.5 and 1.5 Ma (Valla *et al.*, 2012). However, the late-Miocene to Pliocene history of the area remains unclear, with reported rapid exhumation occurring either between 10 and 6 Ma (Vernon *et al.*, 2009; Valla *et al.*, 2012) or more recently until *c.* 4–3 Ma (Vernon *et al.*, 2009; Valla *et al.*, 2011). Whether these are continuous or separate events remained unresolved by previous thermochronometric investigations.

Our new thermal modelling suggests a three-phase exhumation history of the area. Note that HeFTy and QTQt modelling outcomes may differ slightly with respect to the predicted cooling histories, although their first-order features clearly overlap (Fig. S2): while HeFTy modelling uses the thermochronological information of each individual sample (Figs. 3 and 4), QTQt modelling considers the thermochronological information of the entire dataset to derive a common and thus averaged cooling history (Figs. 5 and S1). This may lead to distinct details in the resulting time–temperature paths for individual samples (Fig. S2). We favour here the QTQt modelling approach, which allows us to reconstruct a regional exhumation history representative of the entire dataset. Rapid late-Miocene exhumation until *c.* 5 Ma appears to be regionally significant, with similar evidence reported in other Alpine ECMs: the Mont-Blanc (Glotzbach *et al.*, 2008, 2011), the Ecrins-Pelvoux (van der Beek *et al.*, 2010), the Aiguilles Rouges (Valla *et al.*, 2012) and the Gotthard (Glotzbach *et al.*, 2010) massifs. This coeval rapid exhumation of the ECMs, concordant with frontal migration of tectonic deformation in the Jura Mountains (Sommaruga, 1999; Becker, 2000), may reflect underplating of normal-thickness continental crust below the

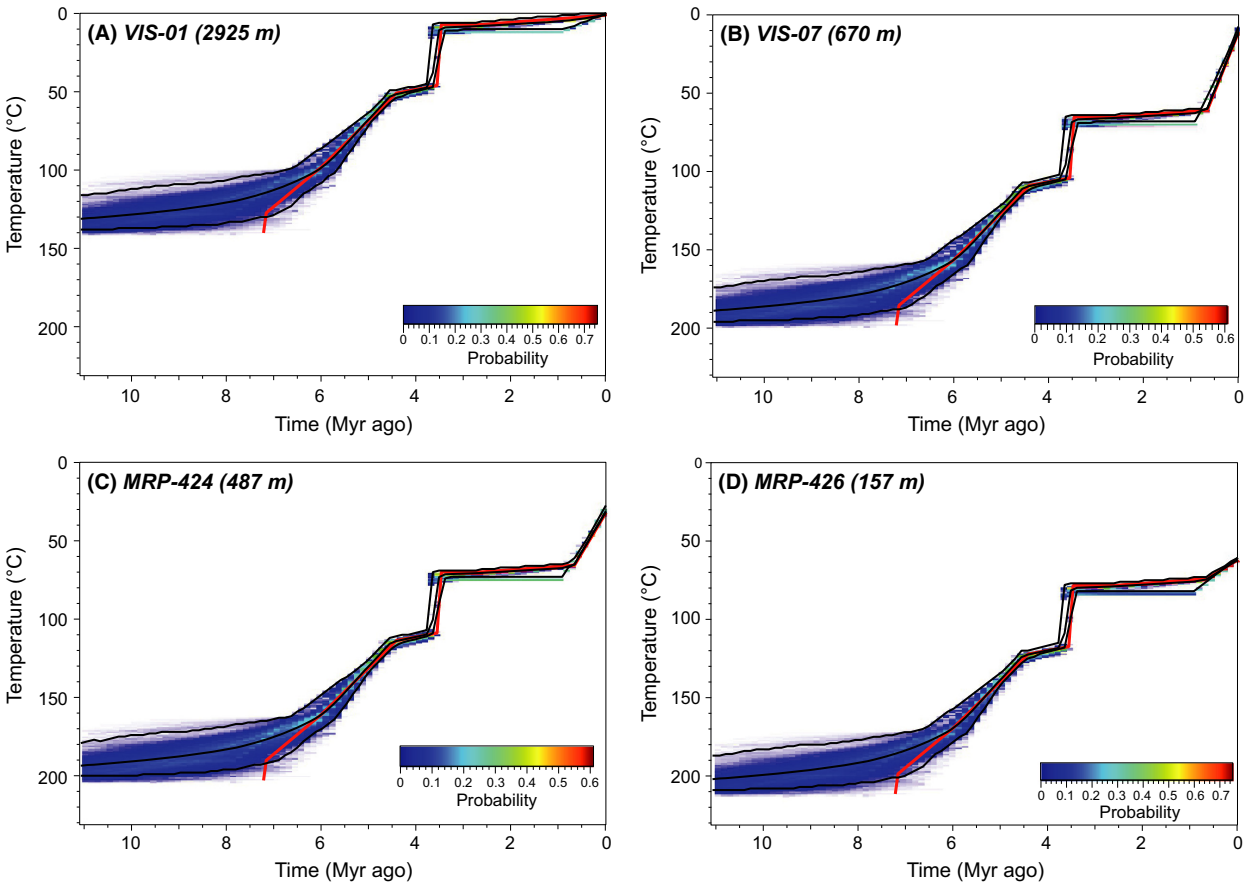

Fig. 5 Selected thermal histories for (A) VIS-01, (B) VIS-07, (C) MRP-424 and (D) MRP-426 from joint thermal modelling of all VIS and MRP samples using QTQt software (Gallagher, 2012). Black lines represent the expected model (weighted mean model) and its 95% confidence intervals; red lines show the maximum-likelihood model (best fitting model). Numerical modelling was run for 3×10^{5} iterations to ensure model convergence (cf. Fig. S1), including general t–T priors of 6.5±6.5 Ma and 70±70 °C, respectively, no reheating and a shared steady geothermal gradient (general prior of 30±5 °C km^{-1}) except for present-day conditions (measured present-day temperatures as shown in Figs. 3,4). The model converged towards an inferred palaeo-geothermal gradient of ~26–28 °C km^{-1}. See Fig. S1 for model convergence and performance.

ECMs (e.g. Cardello *et al.*, 2015) preceding an overall slow-down of Alpine convergence (Schmid *et al.*, 1996). Our modelling also constrains a subsequent Pliocene (between *c.* 4 and 3 Ma) event of 1–1.2 km exhumation. This short episode is coeval with inversion and thrusting of the northern Alpine foreland basin (Cederbom *et al.*, 2011; von Hagke *et al.*, 2012) and associated with denudation of similar magnitude (1–1.5 km) and duration (<1 Ma, e.g. Yanites *et al.*, 2013), suggesting orogen contraction and reactivation of tectonic deformation in the area following the transition to wetter climatic conditions (Cederbom *et al.*, 2004, 2011) and/or a major drainage reorganisation (Ziegler and Fraefel, 2009; Schlunegger and Mosar, 2011). Pliocene exhumation has also been proposed in adjacent areas of the Aar massif (Reinecker *et al.*, 2008) and Helvetic nappes (Cardello *et al.*, 2015). However, these studies related exhumation to tectonic denudation along the footwall of the RSF (Fig. 1), whereas our compiled data show no age offset (and thus no differential tectonic exhumation) across the RSF and PFT after *c.* 7 Ma (Fig. 6). This suggests that increased exhumation and the proposed tilting of the Aar massif and Helvetic nappes (Reinecker *et al.*, 2008; Cardello *et al.*, 2015) were linked to a more regional but short-lived event. Finally, the late-stage exhumation inferred from QTQt modelling is similar to previous $^{4}He/^{3}He$-derived cooling histories (Valla *et al.*, 2011, 2012), confirming differential exhumation linked to glacial valley carving and relief increase. However, our new data and modelling more tightly constrain the time of onset of glacial valley carving to be at 1 Ma or later (Fig. 5). This timing is coeval with both stratigraphic evidence for major Alpine glaciation in the Po basin (Muttoni *et al.*, 2003) and glacial deepening of the Aare valley (Haeuselmann *et al.*, 2007).

Our data also allow us to discuss the palaeo-geothermal conditions in the area (Fig. 7). The modern geothermal anomaly affecting the area (geothermal gradient >100 °C km^{-1}, Fig. 7B) has been ascribed to topography-driven fluid circulation from high elevations within the fractured Aar massif (Kloos, 2004). The local resurgence at low elevations is probably bound to the PFT (Fig. 7A), suggesting long-lived fluid circulation associated with this tectonic structure (Kloos, 2004). However, this geothermal anomaly is not evidenced in our thermochronometric dataset. Averaged shorter and more dispersed TL distributions for MRP samples (Fig. 2) may be interpreted as evidence for partial resetting due to elevated temperatures, although the relatively low number of measured track lengths may bias the TL distributions. AFT and AHe ages, however, show neither significant younging in the borehole nor curved age–elevation relationships indicative of geothermal perturbation. HeFTy modelling confirms that thermal perturbations have been limited for these samples. Although thermal constraints for the borehole samples allow potential heating into the partial annealing zone during the last 1 Myr, modelling outcomes show maximum reheating below 60 °C (Fig. 4), in agreement with a maximum reservoir temperature of <110 °C from geothermometry (Kloos, 2004). Our QTQt modelling results also suggest that this geothermal anomaly has not been long-lived, predicting a palaeo-geothermal gradient of ~26–28 °C km^{-1} until *c.* 1 Ma, in agreement with the best estimate of palaeo-geothermal gradients from HeFTy modelling (Fig. S4), previous thermal modelling of $^{4}He/^{3}He$ data (Valla *et al.*, 2011) and measurements of the present-day gradient within the Aar massif away from geothermal anomalies (Fig. 7). We thus suggest that glacial topographic relief increase could have reinforced lateral variations in hydrostatic pressure (Ehlers, 2005), driving fluid flow from high elevations to valley bottoms in the fractured Aar massif (Fig. 7A). Hydrothermal circulation and associated geothermal anomalies may have varied during the Quaternary: glacial conditions reduce hydrothermal activity by limiting fluid percolation at high elevations (Maréchal *et al.*, 1999) and decreasing pressure gradients by ice-filling of valleys (Thiébaud *et al.*, 2010). This suggests that the modern high geothermal gradients at the Brigerbad borehole represent transient conditions linked to post-glacial heat evacuation (e.g. Gallino *et al.*, 2009), which explains the minor influence on our thermochronometric data.

Conclusions

We used low-temperature thermochronometry on surface and

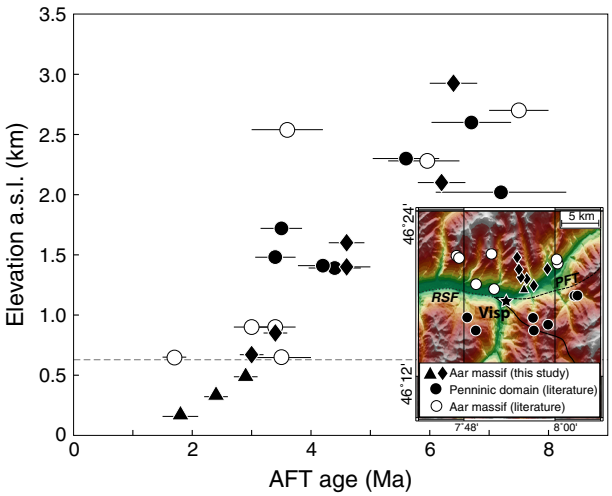

Fig. 6 Age–elevation profile combining VIS and MRP data (black diamonds and triangles, respectively) with literature AFT ages for the Visp-Brigerbad area (black and open circles; Wagner *et al.*, 1977; Soom, 1990; Reinecker *et al.*, 2008). Inset shows sample locations. Black circles indicate samples located south of the Rhône-Simplon fault (RSF) and the Penninic Frontal Thrust (PFT). No age offset is observed between samples from the hangingwall and the footwall of the RSF/PFT, indicating no significant vertical offset along these tectonic structures after AFT system closure (i.e. since ~7 Ma).

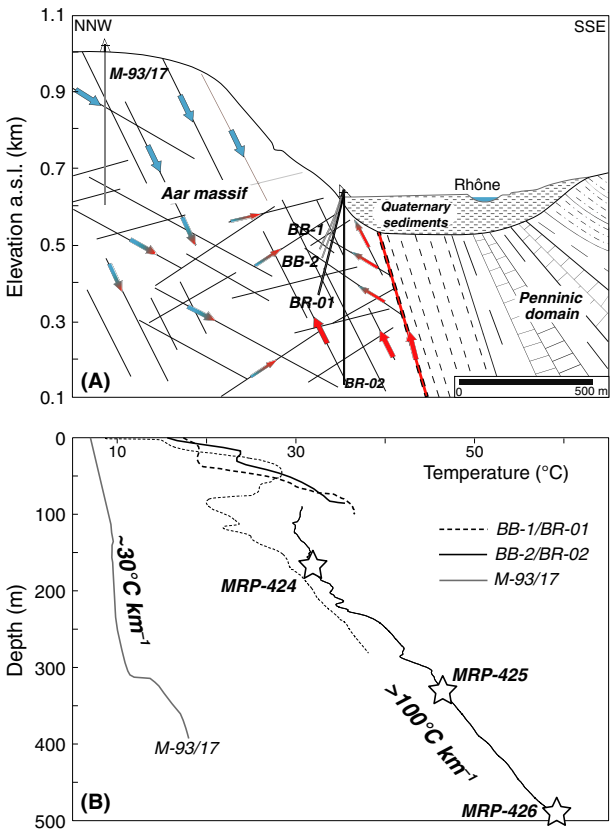

Fig. 7 Schematic geological cross-section and geothermal activity. (A) Valley cross-section with major litho-tectonic units (after Schmid *et al.*, 2004) and location of geothermal exploration boreholes at Brigerbad (BB-1 and -2, BR-01 and -02) and in the Aar massif (M-93/17) (after Kloos, 2004; Alpgéo/Norbert, 2011). Coloured arrows represent inferred fluid circulation within the fractured Aar massif and along the Penninic Frontal Thrust (see Figs. 1 and 2A for location). (B) Present-day measured geothermal gradients (Alpgéo/Norbert, 2011) within different boreholes (see Fig. 7A for location). Open stars show MRP sample locations along the BR-02 borehole.

borehole samples in the Aar massif to derive tight temporal constraints on the exhumation history of the area. Thermal modelling reveals three distinct exhumation events since the late Neogene. Late-Miocene exhumation appears to have been tectonically driven by crustal underplating below the External Crystalline Massifs; this was followed by a Pliocene regional exhumation pulse, which we suggest was the orogen's response to wetter climatic conditions and/or drainage reorganisation. Following previous studies, we finally show that Quaternary exhumation has been driven by glacial valley carving since *c.* 1 Ma or later, potentially triggering local and short-lived hydrothermal activity.

Acknowledgements

We thank T. Ehlers, A. Kounov, an anonymous reviewer and the associate editor for their constructive comments. We also thank K. Gallagher for help with QTQt modelling, M. Buser and P. Hayoz for access to borehole reports and samples, A. Kounov for access to FT facilities at Basel University and N. Fylstra for help with AHe dating. We thank G. Bianchetti (Alpgéo) and J. Jacquod (Norbert SA) for sharing useful borehole information. P.G.V. acknowledges funding from the SNSF (grant Ambizione PZ00P2_148191) and the ETH-Zürich COFUND. D.L.S. acknowledges the Ann and Gordon Getty Foundation and the France Berkeley Fund.

References

Alpgéo/Norbert, 2011. Geothermie Brigerbad - Phase II, Forages Géothermiques 08-BR1 & 10-BR2: Rapport géologique et hydrogéologique. A l'attention de PG Géothermie Brig-Glis, 35 pp.

Baran, R., Friedrich, A.M. and Schlunegger, F., 2014. The late Miocene to Holocene erosion pattern of the Alpine foreland basin reflects Eurasian slab unloading beneath the western Alps rather than global climate change. *Lithosphere*, **6**, 124–131.

Becker, A., 2000. The Jura Mountains - An active foreland fold-and-thrust belt? *Tectonophysics*, **321**, 381–406.

Braun, J., 2002. Quantifying the effect of recent relief changes on age elevation relationships. *Earth Planet. Sci. Lett.*, **200**, 331–343.

Campani, M., Mancktelow, N., Seward, D., Rolland, Y., Muller, W. and Guerra, I., 2010. Geochronological evidence for continuous exhumation through the ductile-brittle transition along a crustal-scale low-angle normal fault: Simplon Fault Zone, Central Alps. *Tectonics*, **29**, TC3002.

Campani, M., Mulch, A., Kempf, O., Schlunegger, F. and Mancktelow, N., 2012. Miocene paleotopography of the Central Alps. *Earth Planet. Sci. Lett.*, **337**, 174–185.

Cardello, G.L., Almqvist, B.S.G., Hirt, A.M. and Mancktelow, N.S., 2015. Determining the timing of formation of the Rawil Depression in the Helvetic Alps by palaeomagnetic and structural methods. *Geol. Soc. London Spec. Publ.*, **425**, doi: 10.1144/SP425.4.

Cederbom, C., Sinclair, H., Schlunegger, F. and Rahn, M., 2004. Climate induced rebound and exhumation of the European Alps. *Geology*, **32**, 709–712.

Cederbom, C.E., van der Beek, P.A., Schlunegger, F., Sinclair, H.D. and Oncken, O., 2011. Rapid extensive erosion of the North Alpine foreland basin at 5-4 Ma. *Basin Res.*, **23**, 528–550.

Champagnac, J.-D., Sue, C., Delacou, B. and Burkhard, M., 2004. Brittle deformation in the inner NW Alps: from early orogen-parallel extrusion to late orogen-perpendicular collapse. *Terra Nova*, **16**, 232–242.

Champagnac, J.-D., Molnar, P., Anderson, R.S., Sue, C. and Delacou, B., 2007. Quaternary erosion-induced isostatic rebound in the western Alps. *Geology*, **35**, 195–198.

Champagnac, J.-D., Schlunegger, F., Norton, K., von Blanckenburg, F., Abbühl, L.M. and Schwab, M., 2009. Erosion-driven uplift of the modern Central Alps. *Tectonophysics*, **474**, 236–249.

Dempster, T.J. and Persano, C., 2006. Low temperature thermochronology;

resolving geotherm shapes or denudation histories? *Geology*, **34**, 73–76.
Densmore, M.S., Ehlers, T.A. and Woodsworth, G.J., 2007. Effect of alpine glaciation on thermochronometer age-elevation profiles. *Geophys. Res. Lett.*, **34**, L02502.
Ehlers, T.A., 2005. Crustal thermal processes and the interpretation of thermochronometer data. *Rev. Mineral. Geochem.*, **58**, 315–350.
Farley, K.A., Wolf, R.A. and Silver, L.T., 1996. The effects of long alpha-stopping distances on (U-Th)/He ages. *Geochim. Cosmochim. Acta*, **60**, 4223–4229.
Finckh, P. and Frei, W., 1991. Seismic reflection profiling in the Swiss Rhone valley, Part 1: Seismic reflection field work, seismic processing and seismic results of the Roche-Vouvry and Turtmann and Agarn lines. *Eclogae Geol. Helv.*, **84**, 345–357.
Flowers, R.M., Ketcham, R.A., Shuster, D.L. and Farley, K.A., 2009. Apatite (U-Th)/He thermochronometry using a radiation damage accumulation and annealing model. *Geochim. Cosmochim. Acta*, **73**, 2347–2365.
Fox, M., Herman, F., Kissling, E. and Willett, S.D., 2015. Rapid exhumation in the Western Alps driven by slab detachment and glacial erosion. *Geology*, **43**, 379–382.
Galbraith, R.F. and Laslett, G.M., 1993. Statistical models for mixed fission-track ages. *Nucl. Tracks Radiat. Meas.*, **21**, 459–470.
Gallagher, K., 2012. Transdimensional inverse thermal history modeling for quantitative thermochronology. *J. Geophys. Res.*, **117**, B02408.
Gallagher, K., Brown, R. and Johnson, C., 1998. Fission track analysis and its applications to geological problems. *Annu. Rev. Earth Planet. Sci.*, **26**, 519–572.
Gallino, S., Josnin, J.-Y., Dzikowski, M., Cornaton, F. and Gasquet, D., 2009. The influence of paleoclimatic events on the functioning of an alpine thermal system (France): the contribution of hydrodynamic-thermal modeling. *Hydrogeol. J.*, **17**, 1887–1900.
Glotzbach, C., Reinecker, J., Danisik, M., Rahn, M., Frisch, W. and Spiegel, C., 2008. Neogene exhumation history of the Mont Blanc massif, Western Alps. *Tectonics*, **27**, TC4011.
Glotzbach, C., Reinecker, J., Danisik, M., Rahn, M., Frisch, W. and Spiegel, C., 2010. Thermal history of the central Gotthard and Aar massifs (European Alps): Evidence for steady state, long-term exhumation. *J. Geophys. Res.*, **115**, F03017.
Glotzbach, C., van der Beek, P.A. and Spiegel, C., 2011. Episodic exhumation of the Mont Blanc massif, Western Alps: Constraints from numerical modelling of thermochronology data. *Earth Planet. Sci. Lett.*, **304**, 417–430.
Gorynski, K.E., Walker, J.D., Stockli, D.F. and Sabin, A., 2014. Apatite (U-Th)/He thermochronometry as an innovative geothermal exploration tool: A case study from the southern Wassuk Range, Nevada. *J. Volcanol. Geoth. Res.*, **270**, 99–114.
Haeuselmann, P., Granger, D.E., Jeannin, P.-Y. and Lauritzen, S.-E., 2007. Abrupt glacial valley incision at 0.8 Ma dated from cave deposits in Switzerland. *Geology*, **35**, 143–146.
von Hagke, C., Cederbom, C.E., Oncken, O., Stöckli, D.F., Rahn, M.K. and Schlunegger, F., 2012. Linking the northern Alps with their foreland: The latest exhumation history resolved by low-temperature thermochronology. *Tectonics*, **31**, TC5010.
Hinderer, M., 2001. Late Quaternary denudation of the Alps; valley and lake fillings and modern river loads. *Geodin. Acta*, **14**, 231–263.
Hurford, A.J. and Green, P.F., 1983. The zeta age calibration of fission-track dating. *Chem. Geol.*, **1**, 285–317.
Ketcham, R.A., 2005. Forward and inverse modelling of low-temperature thermochronometry data. *Rev. Mineral. Geochem.*, **58**, 275–314.
Ketcham, R.A., Carter, A.C., Donelick, R.A., Barbarand, J. and Hurford, A.J., 2007a. Improved measurement of fission-track annealing in apatite using *c*-axis projection. *Am. Mineral.*, **92**, 789–798.
Ketcham, R.A., Carter, A.C., Donelick, R.A., Barbarand, J. and Hurford, A.J., 2007b. Improved modelling of fission-track annealing in apatite. *Am. Mineral.*, **92**, 799–810.
Ketcham, R.A., Donelick, R.A., Balestrieri, M.L. and Zattin, M., 2009. Reproducibility of apatite fission-track length data and thermal history reconstruction. *Earth Planet. Sci. Lett.*, **284**, 504–515.
Ketcham, R.A., Gautheron, C. and Tassan-Got, L., 2011. Accounting for long alpha-particle stopping distances in (U-Th-Sm)/He geochronology: Refinement of the baseline case. *Geochim. Cosmochim. Acta*, **75**, 7779–7791.
Kloos, O., 2004. Hydrochimie et Hydrogéologie des sources thermales de Brigerbad (VS). Diploma thesis, University of Neuchâtel (Switzerland), 89 pp.
Kuhlemann, J., Frisch, W., Székely, B., Dunkl, I. and Kázmér, M., 2002. Post-collisional sediment budget history of the Alps: Tectonic versus climatic control. *Int. J. Earth Sci.*, **91**, 818–837.
Kühni, A. and Pfiffner, O.A., 2001. Drainage patterns and tectonic forcing: a model study for the Swiss Alps. *Basin Res.*, **13**, 169–197.
Mahéo, G., Gautheron, C., Leloup, P., Fox, M., Tassant-Got, L. and Douville, E., 2012. Neogene exhumation history of the Bergell massif (southeast Central Alps). *Terra Nova*, **25**, 110–118.
Mancktelow, N., 1985. The Simplon Line: A major displacement zone in the Western Lepontine Alps. *Eclogae Geol. Helv.*, **78**, 73–96.
Mancktelow, N.S., 1992. Neogene lateral extension during convergence in the central Alps: Evidence from interrelated faulting and backfolding around the Simplon Pass (Switzerland). *Tectonophysics*, **215**, 295–317.
Maréchal, J.-C., Perochet, P. and Tacher, L., 1999. Long-term simulations of thermal and hydraulic characteristics in a mountain massif: The Mont Blanc case study, French and Italian Alps. *Hydrogeol. J.*, **7**, 341–354.
Molnar, P. and England, P., 1990. Late Cenozoic uplift of mountain ranges and global climate change: chicken or egg? *Nature*, **346**, 29–34.
Muttoni, G., Carcano, C., Garzanti, E., Ghielmi, M., Piccin, A., Pini, R., Rogledi, S. and Sciunnach, D., 2003. Onset of major Pleistocene glaciations in the Alps. *Geology*, **31**, 989–992.
Nocquet, J.-M. and Calais, E., 2004. Geodetic measurements of crustal deformation in the Western Mediterranean and Europe. *Pure Appl. Geophys.*, **161**, 661–681.
Norton, K.P., Abbühl, L.M. and Schlunegger, F., 2010. Glacial conditioning as an erosional driving force in the Central Alps. *Geology*, **38**, 655–658.
Olen, S., Ehlers, T.A. and Densmore, M.S., 2012. Limits to reconstructing paleotopography from thermochronometer data. *J. Geophys. Res.*, **117**, F01024.
Persaud, M. and Pfiffner, O.A., 2004. Active deformation in the eastern Swiss Alps: Post-glacial faults, seismicity and surface uplift. *Tectonophysics*, **385**, 59–84.
Raymo, M.W. and Ruddiman, W.F., 1992. Tectonic forcing of late Cenozoic climate. *Nature*, **359**, 117–122.
Reinecker, J., Danišík, M., Schmid, C., Glotzbach, C., Rahn, M., Frisch, W. and Spiegel, C., 2008. Tectonic control on the late stage exhumation of the Aar Massif (Switzerland): Constraints from apatite fission track and (U-Th)/He data. *Tectonics*, **27**, TC6009.
Roe, G.H., Whipple, K.X. and Fletcher, J.K., 2008. Feedbacks among climate, erosion, and tectonics in a critical wedge orogeny. *Am. J. Sci.*, **308**, 815–842.
Rosselli, A. and Olivier, R., 2003. Modélisation gravimétrique 2.5D et

cartes isohypses au 1:100'000 du substratum rocheux de la Vallée du Rhône entre Villeneuve et Brig (Suisse). *Eclogae Geol. Helv*., **96**, 399–423.
Schlatter, A., 2014. Kinematische Gesamtausgleichung der Schweizer Landesnivellementlinien 2013 und Detaildarstellung der rezenten vertikalen Oberflächenbewegungen in der Zentralschweiz. Nagra Arbeitsbericht NAB 14-38, 11 pp.
Schlunegger, F. and Mosar, J., 2011. The last erosional stage of the Molasse Basin and the Alps. *Int. J. Earth Sci*., **100**, 1147–1162.
Schmid, S.M., Pfiffner, O.A., Froitzheim, N., Schönborn, G. and Kissling, E., 1996. Geophysical geological transect and tectonic evolution of the Swiss-Italian Alps. *Tectonics*, **15**, 1036–1064.
Schmid, S.M., Fügenschuh, B., Kissling, E. and Schuster, R., 2004. Tectonic map and overall architecture of the Alpine orogen. *Eclogae Geol. Helv*., **97**, 93–117.
Seward, D. and Mancktelow, N.S., 1994. Neogene kinematics of the central and Western Alps: Evidence from fission-track dating. *Geology*, **22**, 803–806.
Shuster, D.L., Flowers, R.M. and Farley, K.A., 2006. The influence of natural radiation damage on helium diffusion kinetics in apatite. *Earth Planet. Sci. Lett*., **249**, 148–161.
Sommaruga, A., 1999. Decollement tectonics in the Jura foreland fold-and-thrust belt. *Mar. Pet. Geol*., **16**, 111–134.
Sonney, R. and Vuataz, F.D., 2008. Properties of geothermal fluids in Switzerland: a new interactive database. *Geothermics*, **37**, 496–509.
Sonney, R. and Vuataz, F.D., 2009. Numerical modelling of Alpine deep flow systems: a management and prediction tool for an exploited geothermal reservoir (Lavey-les-Bains, Switzerland). *Hydrogeol. J*., **17**, 601–616.
Soom, M.A., 1990. Abkühlungs- und Hebungsgeschichte der Externmassive und der penninischen Decken beidseits der Simplon-Rhone-Linie seit dem Oligozän: Spaltspurdatierung an Apatit/Zirkon und K-Ar-Datierungen an Biotit/Muskovit (westliche Zentralalpen). PhD thesis, University of Bern (Switzerland), 64 pp.
Stüwe, K., White, L. and Brown, R.W., 1994. The influence of eroding topography on steady state isotherms. Application to fission track analysis. *Earth Planet. Sci. Lett*., **124**, 63–74.
Thiébaud, E., Gallino, S., Dzikowski, M. and Gasquet, G., 2010. The influence of glaciations on the dynamics of mountain hydrothermal systems: numerical modeling of the La Léchère system (Savoie, France). *Bull. Soc. Géol. Fr*., **181**, 295–304.
Tremblay, M.M., Fox, M., Schmidt, J.L., Tripathy-Lang, A., Wielicki, M.M., Harrison, T.M., Zeitler, P.K. and Shuster, D.L., 2015. Erosion in southern Tibet shut down at ~10 Ma due to enhanced rock uplift within the Himalaya. *Proc. Natl Acad. Sci*., **112**, 12030–12035.
Valla, P.G., Herman, F., van der Beek, P.A. and Braun, J., 2010. Inversion of thermochronological age-elevation profiles to extract independent estimates of denudation and relief history - I: Theory and conceptual model. *Earth Planet. Sci. Lett*., **295**, 511–522.
Valla, P.G., Shuster, D.L. and van der Beek, P.A., 2011. Major increase in relief of the European Alps during mid-Pleistocene glaciations recorded by apatite $^{4}He/^{3}He$ thermochronometry. *Nat. Geosci*., **4**, 688–692.
Valla, P.G., van der Beek, P.A., Shuster, D.L., Braun, J., Herman, F., Tassan-Got, L. and Gautheron, C., 2012. Late Neogene exhumation and relief development of the Aar and Aiguilles Rouges massifs (Swiss Alps) from low-temperature thermochronology modelling and $^{4}He/^{3}He$ thermochronometry. *J. Geophys. Res*., **117**, F01004.
van der Beek, P.A., Valla, P.G., Herman, F., Braun, J., Persano, C., Dobson, K.J. and Labrin, E., 2010. Inversion of thermochronological age elevation profiles to extract independent estimates of denudation and relief history-II: Application to the French Western Alps. *Earth Planet. Sci. Lett*., **296**, 9–22.
Vernon, A.J., van der Beek, P.A., Sinclair, H.D. and Rahn, M.K., 2008. Increase in late Neogene denudation of the European Alps confirmed by analysis of a fission track thermochronology database. *Earth Planet. Sci. Lett*., **270**, 316–329.
Vernon, A.J., van der Beek, P.A., Sinclair, H.D., Persano, C., Foeken, J. and Stuart, F.M., 2009. Variable late Neogene exhumation of the central European Alps: Low-temperature thermochronology from the Aar Massif, Switzerland, and the Lepontine Dome, Italy. *Tectonics*, **28**, TC5004.
Wagner, G.A., Reimer, G.M. and Jäger, E., 1977. Cooling ages derived by apatite fission track, mica Rb-Sr and K-Ar dating: The uplift and cooling history of the central Alps. *Inst. Geol. Mineral. Univ. Padova Mem*., **30**, 1–27.
Whipp, D.M. and Ehlers, T.A., 2007. Influence of groundwater flow on thermochronometer-derived exhumation rates in the central Nepalese Himalaya. *Geology*, **35**, 851–854.
Whipple, K.X., 2009. The influence of climate on the tectonic evolution of mountain belts. *Nat. Geosci*., **2**, 97–104.
Whipple, K.X. and Meade, B.J., 2006. Orogen response to changes in climatic and tectonic forcing. *Earth Planet. Sci. Lett*., **243**, 218–228.
Willett, S., 2010. Late Neogene erosion of the Alps: A climate driver? *Annu. Rev. Earth Planet. Sci*., **38**, 411–437.
Willett, S.D. and Brandon, M.T., 2002. On steady states in mountain belts. *Geology*, **30**, 175–178.
Willett, S.D., Schlunegger, F. and Picotti, V., 2006. Messinian climate change and erosional destruction of the central European Alps. *Geology*, **34**, 613–616.
Yanites, B.J., Ehlers, T.A., Becker, J.K., Schnellmann, M. and Heuberger, S., 2013. High magnitude and rapid incision from river capture: Rhine River, Switzerland. *J. Geophys. Res*., **118**, 1060–1084.
Ziegler, P.A. and Fraefel, M., 2009. Response of drainage systems to Neogene evolution of the Jura fold-thrust belt and Upper Rhine Graben. *Swiss J. Geosci*., **102**, 57–75.

Received 8 December 2015; revised version accepted 19 July 2016

Supporting Information

Additional Supporting Information may be found in the online version of this article:

Figure S1. Thermal modelling combining all VIS and MRP samples in QTQt software (Gallagher, 2012).

Figure S2. Comparison of modelled time-temperature paths between HeFTy (grey and white lines) and QTQt (expected model in Fig. S1A, coloured envelope) for VIS-01 (A), VIS-07 (B), MRP-424 (C) and MRP-426 (D) samples.

Figure S3. Thermochronometric information within the APAZ obtained from HeFTy thermal modelling (Figs. 3,4).

Figure S4. Composite cooling histories of the Visp-Brigerbad region from AFT and TL information (Fig. S3, light grey envelopes show samples with <50 measured TL, i.e. VIS-05 and -07, MRP-425 and -426), considering shared cooling history and geothermal gradient between all VIS and MRP samples.

